Proline 107 Is a Major Determinant in Maintaining the Structure of the Distal Pocket and Reactivity of the High-Spin Heme of MauG

ARTICLE *in* BIOCHEMISTRY · FEBRUARY 2012

Impact Factor: 3.02 · DOI: 10.1021/bi201882e · Source: PubMed

7 AUTHORS, INCLUDING:

Manliang Feng
Tougaloo College
20 PUBLICATIONS **430** CITATIONS
SEE PROFILE

Erik T Yukl
New Mexico State University
24 PUBLICATIONS **516** CITATIONS
SEE PROFILE

Aimin Liu
Georgia State University
79 PUBLICATIONS **1,277** CITATIONS
SEE PROFILE

Victor L Davidson
University of Central Florida
219 PUBLICATIONS **5,294** CITATIONS
SEE PROFILE

Published in final edited form as:
Biochemistry. 2012 February 28; 51(8): 1598–1606. doi:10.1021/bi201882e.

Proline 107 is a major determinant in maintaining the structure of the distal pocket and reactivity of the high-spin heme of MauG

Manliang Feng[1], **Lyndal M. R. Jensen**[2,#], **Erik T. Yukl**[2,#], **Xiaoxi Wei**[3], **Aimin Liu**[3], **Carrie M. Wilmot**[2], and **Victor L. Davidson**[4]

[1]Department of Chemistry, Tougaloo College, Tougaloo, MS 39174

[2]Department of Biochemistry, Molecular Biology and Biophysics, University of Minnesota, Minneapolis, MN 55455

[3]Department of Chemistry, Georgia State University, P.O. Box 4098, Atlanta, GA, 30303

[4]Burnett School of Biomedical Sciences, College of Medicine, University of Central Florida, Orlando, FL 32827

Abstract

The diheme enzyme MauG catalyzes a six-electron oxidation required for posttranslational modification of a precursor of methylamine dehydrogenase (preMADH) to complete the biosynthesis of its protein-derived tryptophan tryptophylquinone (TTQ) cofactor. Crystallographic studies had shown that Pro107, which resides in the distal pocket of the high-spin heme of MauG, changes conformation upon binding of CO or NO to the heme iron. In this study, Pro107 was converted to Cys, Val and Ser by site-directed mutagenesis. The structures of each of these MauG mutant proteins in complex with preMADH were determined, as were their physical and catalytic properties. P107C MauG was inactive and the crystal structure revealed that Cys107 had been oxidatively modified to a sulfinic acid. Mass spectrometry revealed that this modification was present prior to crystallization. P107V MauG exhibited spectroscopic and catalytic properties that were similar to wild-type MauG, but P107V MauG was more susceptible to oxidative damage. The P107S mutation caused a structural change which resulted in the five-coordinate high-spin heme being converted to a six-coordinate heme with a distal axial ligand provided by Glu113. EPR and resonance Raman spectroscopy revealed this heme remained high-spin but with much increased rhombicity as compared to the axial signal of wild-type MauG. P107S MauG was resistant to reduction by dithionite and reaction with H_2O_2, and unable to catalyze TTQ biosynthesis. These results show that the presence of Pro107 is critical in maintaining the proper structure of the distal heme pocket of the high-spin heme of MauG, enabling exogenous ligands to bind and directing the reactivity of the heme-activated oxygen during catalysis, thus minimizing the oxidation of other residues of MauG.

MauG is a di-*c*-type heme enzyme (1) responsible for the posttranslational modification of methylamine dehydrogenase (MADH) (2) that generates the protein-derived cofactor (2–4), tryptophan tryptophylquinone (TTQ) (5). In MADH from *Paracoccus denitrificans*, TTQ is formed from residues βTrp57 and βTrp108 (6). The substrate for this reaction is a monohydroxylated precursor (preMADH) where one oxygen atom has been inserted into the

‡Address correspondence to: Victor L. Davidson, Burnett School of Biomedical Sciences, College of Medicine, University of Central Florida, 6900 Lake Nona Blvd., Orlando, FL 32827 Tel: 407-266-7111. Fax: 407-266-7002. victor.davidson@ucf.edu.
#These authors contributed equally to this work.

‡Coordinates and structure factors have been deposited in the Protein Data Bank 3SVW (P107V MauG/preMADH), 3SJL (P107S MauG/preMADH), and 3SLE (P107C MauG/preMADH).

indole ring of βTrp57 (7, 8). Maturation of the TTQ cofactor is a six-electron oxidation process comprised of three 2-electron oxidations; insertion of the second OH group into βTrp57, formation of the crosslink between βTrp57 and βTrp108, and oxidation of the quinol to quinone. These two-electron oxidation reactions require the formation of a high-valent *bis*-Fe(IV) MauG intermediate (9) in which one heme is present as Fe(IV)=O with an axial ligand provided by a His and the other is present as Fe(IV) with His-Tyr axial ligation and no exogenous ligand. This redox state is stabilized even though the two heme irons are separated by 21.1 Å.

The crystal structure of MauG in complex with preMADH (10) revealed that the residues which are modified to form TTQ do not make direct contact with either heme of MauG and therefore the biosynthetic redox reactions within the protein complex require long range electron transfer. The shortest distance between βTrp108 of preMADH and the iron of the oxygen-binding five-coordinate heme is 40.1 Å, and the closest distance to the iron of the six-coordinate heme is 19.4 Å. The crystallized complex is catalytically active as it was demonstrated that addition of H_2O_2 to the protein crystal resulted in formation of mature TTQ within preMADH (10). Recently, mutation of Trp199 of MauG which resides at the MauG-preMADH interface revealed that a hopping mechanism of electron transfer via this residue was required for MauG-dependent biosynthesis of TTQ from preMADH (11).

The crystal structure of the MauG-preMADH complex also revealed interesting features of the two heme sites. As stated earlier, the six-coordinate heme exhibits His-Tyr ligation which is unique for a *c*-type heme. This inspired a subsequent study which showed that mutation of the ligand Tyr294 to His led to a His-His ligated heme, and abolished TTQ biosynthesis in preMADH (12). Rather than stabilizing a *bis*-Fe(IV) state, Y294H MauG formed a compound I-like intermediate. It was concluded that this was not sufficient to support biosynthesis because the required electron transfer was now from preMADH to the five-coordinate heme iron (40.1 Å) rather than the closer six-coordinate heme iron (19.4 Å).

A noteworthy feature of the open distal heme pocket at the high-spin heme site was the presence of residue Pro107. A functional role for this residue was implicated from the crystal structures of CO and NO adducts of MauG in complex with preMADH (13). Pro107 displayed movement when going from the diferrous to the NO- and CO-bound states. Proline side chains can adopt two different conformation states that differ by the sign of their dihedral angles (14). Binding of CO or NO converted Pro107 from one conformation to the other and it was suggested that this conversion represented a mechanism for relieving steric crowding by Pro107. It was also noted that Pro107 might play a steric role in O_2-activation by positioning the distal oxygen atom near the carboxylate of Glu113, which is also perturbed by ligand binding.

In this study Pro107 was mutated to Cys, Val and Ser. These mutations each had different effects on the structure of the heme site, the spectroscopic properties and the reactivity of the hemes. These results describe how Pro107 is critical in maintaining the structure of the distal heme pocket of the five-coordinate heme for proper ligand binding and reactivity.

Materials and methods

Protein expression and purification

Recombinant MauG (1) and MADH (15) were purified from *P. denitrificans* as described previously. PreMADH (16) was expressed in *Rhodobacter sphaeroides* and purified as described previously (17). Pro107 of MauG was converted to Ser, Val, and Cys by site-directed mutagenesis of double-stranded pMEG391 (1), which contains *mau*G, using the Phusion™ site-directed mutagenesis kit. Mutant MauGs were expressed in *P. denitrificans*

and isolated from the periplasmic fraction as described for recombinant wild-type (WT) MauG (1).

Mass Spectrometry

Pro107 mutant MauG proteins were subjected to analysis by mass spectrometry. Samples were desalted and exchanged into 75:25 acetonitrile:water, 0.1% formic acid using C4 resin ZipTip® pipet tips (Millipore) prior to introduction into the mass spectrometer. Data were acquired on a QSTAR XL (AB Sciex) quadrupole time-of-flight mass spectrometer with the IonSpray electrospray source. Samples were manually injected into a 10 μL sample loop plumbed into the divert/inject valve of the instrument. Samples were infused at a flow rate of 10 μL/min with 50:50 acetonitrile:water, 0.1% formic acid. The IonSpray voltage was 4700 volts. The TOF region acceleration voltage was 4 kV and the injection pulse repetition rate was 4.9 kHz. The monoisotopic peaks of human renin substrate tetra-decapeptide from Sigma-Alrdich (St. Louis, MO) were used for external calibration ($[M + 3H]^{3+}$ at 586.9830 and $[M + 2H]^{2+}$ at 879.9705). TOF MS spectra were acquired from 700 – 2200 *m/z* for approximately 5 min with a 1 s accumulation time. The acquisition software was Analyst™ QS v1.0 (AB Sciex). The Bayesian protein reconstruct tool in BioAnalyst™ extensions v1.1 (AB Sciex) was used for multiple charge state data deconvolution of the intact proteins.

Crystallization and X-ray structure determinations of the P107S/V/C MauG-preMADH complexes

A 2:1 Pro107 mutant MauG/preMADH ratio mix corresponding to the stoichiometry observed in the molecular complex of WT MauG/preMADH was used. These protein complexes crystallized through optimization of the conditions previously established for WT MauG/preMADH (10) by hanging drop vapor diffusion in VDX plates (Hampton Research). Single crystals suitable for X-ray data collection were obtained from drops assembled with 1 μL protein solution layered with 3 μL reservoir solution over a 22 % – 26 % w/v PEG 8000, 0.1 M sodium acetate, 0.1 M MES pH 6.4 reservoir. Crystals were cryoprotected as described previously through the inclusion of 10 % PEG 400 (10). X-ray diffraction data were collected at GM/CA-CAT beamlines 23-ID-B and 23-ID-D of the Advanced Photon Source (APS), Argonne National Laboratory, Argonne, IL. Data were collected at 100 K using a beam size matching the dimensions of the largest crystal face. The diffraction data are in the space group *P*1 with one complex (two P107S/V/C MauGs bound to one preMADH) in the asymmetric unit. The data were processed with HKL2000 (18).

Although the space groups of the mutants were triclinic, they were in two different crystal forms distinct from the WT MauG-preMADH *P*1 crystal form. The P107V and P107S MauG-preMADH complexes were isomorphous with each other, but the P107C MauG-preMADH had a different *P*1 cell. Thus, structure solutions were obtained by molecular replacement using PHASER (19) from the CCP4 program suite (20) with the entire WT complex (PDB entry 3L4M) as the search model. Refinement was carried out using REFMAC (21) in the CCP4 program suite (20) and model-building was carried out in COOT (22). Restrained refinement with TLS was carried out using no distance restraints between the heme iron centers and their ligands. Residue 107 of each MauG mutant was well-ordered, and added to the model based on the 2Fo-Fc and Fo-Fc electron density maps. Refinement was assessed as complete when the Fo-Fc electron density contained only noise.

EPR spectroscopy

EPR samples were prepared in 50 mM potassium phosphate buffer, pH 7.4, with 150 μM WT or P107S/V MauG. Continous wave X-band EPR spectra were taken on a Bruker E200 spectrometer at 100-kHz modulation frequency using a dual mode resonator. Temperature

was maintained at 10 K with an ESR910 liquid helium cryostat and an ITC503 temperature controller.

Resonance Raman Spectroscopy

Resonance Raman spectra were recorded using a Raman spectrometer consisting of a Spex model 1877 triple spectrograph and a CCD detector as reported previously (23). A 406.7 nm line from an argon-krypton ion laser (Spectra-Physics BeamLok model 2080-KV) was used as the excitation source, and the Raman signal was collected in a 120° geometry. The laser power was adjusted to ~5 mW at the sample. Each spectrum was recorded with a 60 s accumulation time, and 10 repetitively measured spectra were averaged to improve the quality of the final spectrum. The frequencies of the Raman bands were calibrated using the standard spectra of cyclohexane.

Spectrophotometric assay of TTQ biosynthesis in vitro

Steady-state spectrophotometric assays of MauG-dependent TTQ biosynthesis, using preMADH as a substrate, were performed as described previously (24). The standard assay contained 0.3 μM MauG and varied concentrations of preMADH in 0.01 M potassium phosphate buffer at pH 7.5. The reaction was initiated by the addition of 0.1 mM H_2O_2. TTQ biosynthesis was monitored by the increase in absorbance at 440 nm and the data were fit to eq 1.

$$v/E = k_{cat}[S]/([S]+K_m) \quad (1)$$

Results and Discussion

Crystal structures of the P107 mutant MauG-preMADH complexes

Each of the mutant complexes crystallized in the space group *P*1 with two MauG molecules bound to a single preMADH tetramer in the asymmetric unit. The P107V, P107S and P107C MauG-preMADH crystal structures were solved to 1.86, 1.63 and 2.5 Å resolution, respectively. Although all three mutant structures are in different crystal forms to that of the WT MauG-preMADH crystals, the overall structures are nearly identical to WT with rmsd = 0.22–0.35 Å; the largest deviation belonging to the lower resolution P107C MauG-preMADH structure. Data collection and refinement statistics are presented in Table 1.

Analysis of the P107V MauG-preMADH structure demonstrates that substitution of Pro with Val at position 107 has very little impact on the organization of the high-spin heme distal pocket (Figure 1A and 2A). Val107 occupies a very similar position as Pro in the WT structure, and the positions of distal water molecules are conserved although the mutation causes a modest repositioning of Glu113.

In the P107S MauG-preMADH structure, Glu113 has moved 3.1 Å into the distal pocket to coordinate the heme iron at a Fe-O distance of 2.1 Å (Figure 1B and 2B). The movement of Glu113 disrupts a hydrogen bond between the backbone carbonyl of this residue and the backbone amide of Asp57 (Figure 1C). Asp57 is in a large loop stretching from Ala40 to Tyr72 in the WT structure. In P107S MauG-preMADH, residues 49–62 could not be modeled in either MauG chain suggesting that this region is disordered in the mutant structure. One of the P107V MauG chains can be modeled in this region, although the temperature factors are relatively high. This suggests that the higher disorder of this region in the P107S MauG cannot be solely attributed to the change in crystal form of these two mutants compared to WT, but is at least partially due to the ligation of Glu113 to the heme iron. While not naturally occurring but a result of the P107S mutation, this structure

represents a rare example of axial ligation of a protein bound heme by a Glu. Another example is a cytochrome *c* peroxidase in which the proximal His ligand has been mutated to Glu (25, 26). This differs from P107S MauG in that the proximal His ligand remains unchanged and the Glu ligand is introduced at the distal site as a consequence of a mutation-induced conformational change. Axial Glu coordination to a heme has also been proposed for the cytochrome maturation protein CcmE on the basis of EPR spectroscopy (27).

In the P107C MauG-preMADH structure, refinement of a Cys residue at position 107 resulted in significant positive difference density between it and the heme iron. In order to obtain a satisfactory fit to the density, a cysteine-derived sulfinic acid residue was built in this position (Figure 1D and 2C). The modified residue appears to be coordinating the heme iron through an oxygen atom at a distance of 2.0 Å. Mass spectrometry of P107C MauG confirms that prior to crystallization a +32 mass shift from the predicted mass was present, indicating that cysteine modification is not an artifact of radiation damage. This oxidatively modified residue in close proximity to the oxygen-binding heme illustrates how reactive the intermediates are in the normal catalytic process, and that oxidative damage can occur when the MauG distal pocket structure is perturbed.

Effects of mutation of Pro107 on MauG-dependent TTQ biosynthesis from preMADH

The enzymatic activity of Pro107 mutant MauGs was assayed in a steady-state assay of TTQ biosynthesis with preMADH as substrate and 0.1 mM H_2O_2 as the source of oxidizing equivalents. The kinetic parameters for the reaction with P107V MauG were similar to those reported for WT MauG in the steady state assay with H_2O_2 (28). A comparison is shown in Figure 3 where P107V MauG exhibited a k_{cat} of 0.10 ± 0.01 s^{-1} and a K_m of 1.3 ± 0.1 μM and WT MauG exhibited a k_{cat} of 0.16 ± 0.02 s^{-1} and a K_m of 1.7 ± 0.4 μM (Figure 3). In contrast, under these experimental conditions P107S MauG exhibited no TTQ biosynthesis activity. For the P107C MauG, the ready oxidation of Cys107 to sulfinic acid during overexpression and purification, both of which are performed under aerobic conditions, led to batch-to-batch variation in activity. This ranged from no activity to activity that was quickly lost, even during storage at −80 °C. Given the inability to obtain a homogenous preparation of the unmodified P107C, further investigation of the properties of the Pro107 mutants focused on characterization of P107V MauG and P107S MauG.

Effects of mutation of Pro107 on the absorption spectrum of MauG and reactivity towards dithionite and H_2O_2

The P107V and P107S mutations each had a different effect on the absorption spectrum of the diferric protein (Figure 4). The spectrum of P107V MauG is similar to that of WT MauG in that the Soret peak is centered at 406 nm. However, the Soret peak of P107V MauG is much broader. For P107S MauG the Soret peak is centered at 403 nm and is narrower than that of WT MauG.

The P107V and P107S mutations also each differentially affected the ability to generate the diferrous state of the protein. Reduction of WT MauG is characterized by the red-shift of the Soret peak to 418 nm and the appearance of relatively sharp α and β bands at 550 nm and 520 nm, respectively. The reductive titration of WT MauG with dithionite requires two electron equivalents and reaction with dithionite is very rapid. In contrast, P107S MauG did not react at all after addition of stoichiometric dithionite. In order to obtain a spectrum similar to that of diferrous WT MauG, the addition of 20 equivalents of dithionite was required and took 30 min to complete the spectral change. When the protein was treated with excess ferricyanide to reoxidize the protein it was not possible to regenerate the spectrum of the as-isolated diferric protein indicating that the protein was likely damaged due to the harsher conditions required for reduction. This was also the case for P107V

MauG, but the process required addition of a smaller excess of dithionite and the rate of reduction was much faster. This suggests that displacement of the heme-ligated Glu113 in the P107S mutant is a significant factor in the time taken to achieve reduction, but the damage is primarily the result of requiring a stoichiometric excess of reducing equivalents for reduction, as it occurs in both P107S and P107V MauG. Unfortunately, the inability to achieve efficient reversible reduction of these MauG mutant proteins precluded the possibility of determining the redox potentials for the diferric/diferrous couple.

Reaction of WT MauG with H_2O_2 yields a high-valent *bis*-Fe(IV) species which is evidenced by the decreased intensity and red-shift of the Soret peak. The *bis*-Fe(IV) species forms rapidly (within 2 ms) after addition of stoichiometric H_2O_2 to diferric MauG. In the absence of the preMADH substrate, this high-valent species spontaneously returns to the diferric form in around 10 min. P107V MauG similarly reacts with H_2O_2 rapidly to yield similar spectral changes and shows a spontaneous return to diferric protein with a slight increase of the Soret peak absorbance. In contrast, addition of stoichiometric H_2O_2 to P107S MauG did not cause the spectrum to change. Only when a very large excess of H_2O_2 was added was a spectral change observed, however, it was not characteristic of *bis*-Fe(IV). Instead a very slow decrease of the Soret peak absorbance with no concomitant red-shift was observed, and the species that was formed did not spontaneously return to the initial state. This suggests the need to displace the iron-ligated Glu113 may be impeding the reaction with H_2O_2, as discussed above for the dithionite reduction. The inability of P107S MauG to react with H_2O_2 also provides an explanation for the inability to catalyze TTQ biosynthesis.

Effects of mutation of Pro107 on the EPR spectrum of MauG

The low temperature X-band EPR spectrum of WT MauG exhibits signals from three ferric heme species. A low-spin ($S = 1/2$) heme with g values of 1.87, 2.19, and 2.54, assigned to the His-Tyr ligated heme, accounts for ~50% of the total signal. A high-spin ($S = 5/2$) heme with g values of 1.99 and 5.57, assigned to the five-coordinate His-ligated heme, accounts for ~25% of the total signal. A second broad low-spin heme with g values 1.52, 2.32, and 2.89 is observed which accounts for the remaining 25%. This species has been assigned as a freezing artifact which is derived from approximately half of the high-spin heme upon freezing (10). Whereas the EPR spectrum of diferric P107V MauG presented very similar high- and low-spin heme signals to those observed in the WT MauG spectrum, the EPR spectrum of P107S MauG exhibited features quite different from that of WT MauG (Figure 5). The high-spin ferric signal at $g = 5.57$ in P107S MauG appears to be split into two signals. This feature reflects a much increased rhombicity as compared to the axial signal of WT MauG. The resolved g-values for the high-spin ferric heme are $g_x = 1.99$, $g_y = 5.55$, and $g_z = 6.21$. The low-spin ferric signal assigned to the His-Tyr ligated heme remained the same as seen in WT MauG.

Such an increased rhombicity, as is seen for the high-spin heme in P107S MauG, is typically caused by addition of one or more ligands, and is consistent with the crystal structure of P107S MauG-preMADH that shows monodentate distal ligation by Glu113. Glutamate is considered a weak ligand for a heme iron, and the EPR shows the heme remains high-spin even with the Fe-O distance of 2.1 Å seen in the crystal structure. The broad low-spin ferric EPR signal with g_{max} of 2.89 that was assigned as a freezing artifact in WT MauG is completely absent in the spectrum of P107S MauG. The conversion of high-spin to low-spin heme upon freezing is well documented in di-heme enzymes with some cases leading to complete loss of high-spin ferric signal (29–32). The absence of the freezing artifact in P107S MauG is consistent with a sixth ligand that is difficult to displace and prevents coordination by a stronger internal ligand following a freezing-induced structural change.

Effects of mutation of Pro107 on the resonance Raman spectra MauG

The resonance Raman spectrum of P107V MauG is similar to that of native MauG indicating that this mutation does not induce a significant structural change in the hemes. In contrast, the resonance Raman spectrum of P107S MauG revealed frequency changes in several of the marker bands relative to WT MauG indicating a significant change in the heme structure that is consistent with Glu113 ligation to the heme. The high frequency region of the spectra (Figure 6A) contains several marker bands that are sensitive to oxidation state, spin state and the conformation of the heme macrocycle (33–35). The assignment of marker bands is based on the work of Spiro and coworkers (34). The ν_2 and ν_3 bands of P107S MauG at 1567 and 1472 cm^{-1}, respectively, are from high-spin heme, consistent with the presence of high-spin heme in the EPR spectrum. These ν_2 and ν_3 bands are also shifted to lower frequencies compared with the frequencies of the corresponding high-spin marker bands of WT MauG (1571 and 1478 cm^{-1}, respectively). The frequencies of the ν_2 and ν_3 bands from the low-spin heme, which are somewhat obscured by the high-spin bands, are basically unchanged from those of WT MauG. In the low frequency region (Figure 6B), the δ ($C_\beta C_\alpha S$) mode is shifted from 393 cm^{-1} in WT MauG to 390 cm^{-1} in P107S MauG. The ν_8 mode is also shifted to lower frequency compared to that in the WT MauG. These shifts suggest conformational changes resulting in the thioether bonds to the heme becoming more restrained.

Effects of mutation of Pro107on the susceptibility of MauG to oxidative damage

It was previously shown that WT MauG is inactivated when supplied with oxidation equivalents in the absence of preMADH (36). As discussed above, Cys107 in P107C MauG was oxidized to a sulfinic acid, as evidenced by the crystal structure and analysis by mass spectrometry. As such it was of interest to determine whether the P107V and P107S mutations might also make MauG more susceptible to oxidative damage. To test this, 20 μM MauG was incubated in the presence of 200 μM H_2O_2 for one hour before being quenched by the addition of a small amount of catalase. Each sample was then subjected to ESI-MS (Figure 7). The pattern of oxidation products is different among WT and mutant proteins. WT MauG forms predominantly a single oxidation product with very slow buildup of a second product. In P107V MauG at least three oxidized species are formed and in P107S MauG there appear to be no fewer than six formed with complete loss of the parent peak during the one hour incubation time. As discussed earlier, P107S MauG is unreactive towards stoichiometric H_2O_2 and exhibits an irreversible decrease in absorbance of the Soret peak on addition of excess H_2O_2. The mass spectrometry data indicate that those H_2O_2-induced spectral changes are likely associated with H_2O_2-induced oxidative damage. Thus, each of the mutations of Pro107 makes MauG much more susceptible to oxidative damage.

Conclusions

The results of this study clearly show that the presence of Pro107 is critical in maintaining the proper structure of the distal heme pocket of the high-spin heme of MauG. The structural role of Pro107 seems in large part to be a feature of its size rather than rigidity since P107V MauG reacts with H_2O_2 and exhibits reasonable TTQ biosynthesis activity. However, P107V MauG is more susceptible to oxidative damage than WT MauG. Oxidative damage is also observed for P107C MauG in which Cys107 becomes oxidized to a sulfinic acid. The altered structural and physical properties of P107S MauG demonstrate that Pro107 is not only important for maintaining an open site at the high-spin heme iron to allow binding of exogenous ligands and reactants including H_2O_2, but also to control the reactivity of the activated oxygen so that it is used for long range catalysis, whilst minimizing oxidation of other residues of MauG. Additionally, the P107S MauG results in an unusual structure of a protein-bound heme that is six-coordinate and high-spin with His-Glu axial ligation and unusual spectroscopic properties.

Acknowledgments

This work was supported by NSF Grant MCB-0843537 (A.L.), NIH grants GM-41574 (V.L.D.), GM-66569 (C.M.W.), GM-97779 (E.T.Y) and Minnesota Partnership for Biotechnology and Medical Genomics grant SPAP-05-0013-P-FY06 (C.M.W.).

We thank Professor Hiroyasu Tachikawa for access to the facilities at Jackson State University for resonance Raman studies, Dr. Sheeyong Lee for his participation in the early stages of these studies, Dr. Sooim Shin for helpful discussion and Yu Tang for technical assistance. Computer resources were provided by the Basic Sciences Computing Laboratory of the University of Minnesota Supercomputing Institute, and we thank Can Ergenekan for his support. X-ray data were collected at the Kahlert Structural Biology Laboratory (KSBL) at The University of Minnesota and GM/CA-CAT at the Advanced Photon Source (APS), Argonne National Laboratory, Argonne, IL. GM/CA CAT has been funded in whole or in part with Federal funds from the National Cancer Institute (Y1-CO-1020) and the National Institute of General Medical Science (Y1-GM-1104). Use of the Advanced Photon Source was supported by the U.S. Department of Energy, Basic Energy Sciences, Office of Science, under contract No. DE-AC02-06CH11357. We thank Ed Hoeffner for KSBL support, and the staff at Sector 23, APS for their support.

Abbreviations

MADH	methylamine dehydrogenase
TTQ	tryptophan tryptophylquinone
preMADH	the biosynthetic precursor protein of MADH with incompletely synthesized TTQ
***bis*-Fe(IV) MauG**	redox state of MauG with one heme as Fe(IV)=O and the other as Fe(IV)
WT	wild-type

References

1. Wang Y, Graichen ME, Liu A, Pearson AR, Wilmot CM, Davidson VL. MauG, a novel diheme protein required for tryptophan tryptophylquinone biogenesis. Biochemistry. 2003; 42:7318–7325. [PubMed: 12809487]
2. Davidson VL. Pyrroloquinoline quinone (PQQ) from methanol dehydrogenase and tryptophan tryptophylquinone (TTQ) from methylamine dehydrogenase. Adv Protein Chem. 2001; 58:95–140. [PubMed: 11665494]
3. Davidson VL. Protein-derived cofactors. Expanding the scope of post-translational modifications. Biochemistry. 2007; 46:5283–5292. [PubMed: 17439161]
4. Davidson VL. Generation of protein-derived redox cofactors by posttranslational modification. Mol Biosyst. 2011; 7:29–37. [PubMed: 20936199]
5. McIntire WS, Wemmer DE, Chistoserdov A, Lidstrom ME. A new cofactor in a prokaryotic enzyme: tryptophan tryptophylquinone as the redox prosthetic group in methylamine dehydrogenase. Science. 1991; 252:817–824. [PubMed: 2028257]
6. Chen L, Doi M, Durley RC, Chistoserdov AY, Lidstrom ME, Davidson VL, Mathews FS. Refined crystal structure of methylamine dehydrogenase from *Paracoccus denitrificans* at 1.75 Å resolution. J Mol Biol. 1998; 276:131–149. [PubMed: 9514722]
7. Pearson AR, De La Mora-Rey T, Graichen ME, Wang Y, Jones LH, Marimanikkupam S, Agger SA, Grimsrud PA, Davidson VL, Wilmot CM. Further insights into quinone cofactor biogenesis: probing the role of mauG in methylamine dehydrogenase tryptophan tryptophylquinone formation. Biochemistry. 2004; 43:5494–5502. [PubMed: 15122915]
8. Wang Y, Li X, Jones LH, Pearson AR, Wilmot CM, Davidson VL. MauG-dependent in vitro biosynthesis of tryptophan tryptophylquinone in methylamine dehydrogenase. J Am Chem Soc. 2005; 127:8258–8259. [PubMed: 15941239]

9. Li X, Fu R, Lee S, Krebs C, Davidson VL, Liu A. A catalytic di-heme bis-Fe(IV) intermediate, alternative to an Fe(IV)=O porphyrin radical. Proc Natl Acad Sci USA. 2008; 105:8597–8600. [PubMed: 18562294]
10. Jensen LM, Sanishvili R, Davidson VL, Wilmot CM. In crystallo posttranslational modification within a MauG/pre-methylamine dehydrogenase complex. Science. 2010; 327:1392–1394. [PubMed: 20223990]
11. Abu Tarboush N, Jensen LMR, Yukl ET, Geng J, Liu A, Wilmot CM, Davidson VL. Mutagenesis of tryptophan199 suggets that hopping is required for MauG-dependent tryptophan tryptophylquinone biosynthesis. Proc Natl Acad Sci U S A. 2011; 108:16956–16961. [PubMed: 21969534]
12. Abu Tarboush N, Jensen LM, Feng M, Tachikawa H, Wilmot CM, Davidson VL. Functional importance of tyrosine 294 and the catalytic selectivity for the bis-Fe(IV) state of MauG revealed by replacement of this axial heme ligand with histidine. Biochemistry. 2010; 49:9783–9791. [PubMed: 20929212]
13. Yukl ET, Goblirsch BR, Davidson VL, Wilmot CM. Crystal structures of CO and NO adducts of MauG in complex with pre-methylamine dehydrogenase: Implications for the mechanism of dioxygen activation. Biochemistry. 2011; 50:2931–2938. [PubMed: 21355604]
14. Nemethy G, Gibson KD, Palmer KA, Yoon CN, Paterlini G, Zagari A, Rumsey S, Scheraga HA. Energy parameters in polypeptides. 10 Improved geometrical parameters and nonbonded interactions for use in the ECEPP/3 algorithm, with application to proline-containing peptides. J Phys Chem. 1992; 96:6472–6484.
15. Davidson VL. Methylamine dehydrogenases from methylotrophic bacteria. Methods Enzymol. 1990; 188:241–246. [PubMed: 2126329]
16. Pearson AR, de la Mora-Rey T, Graichen ME, Wang Y, Jones LH, Marimanikkupam S, Aggar SA, Grimsrud PA, Davidson VL, Wilmot CW. Further insights into quinone cofactor biogenesis: Probing the role of MauG in methylamine dehydrogenase TTQ formation. Biochemistry. 2004; 43:5494–5502. [PubMed: 15122915]
17. Graichen ME, Jones LH, Sharma BV, van Spanning RJ, Hosler JP, Davidson VL. Heterologous expression of correctly assembled methylamine dehydrogenase in Rhodobacter sphaeroides. J Bacteriol. 1999; 181:4216–4222. [PubMed: 10400578]
18. Otwinowski Z, Minor W. Processing of X-ray diffraction data collected in oscillation mode. Methods Enzymol. 1997; 276:307–326.
19. McCoy AJ, Grosse-Kunstleve RW, Adams PD, Winn MD, Storoni LC, Read RJ. Phaser crystallographic software. J Appl Crystallogr. 2007; 40:658–674. [PubMed: 19461840]
20. CCP4. Collaborative Computational Project Number 4. Acta Crystallogr Sect D Biol Crystallogr. 1994; 50:760–763. [PubMed: 15299374]
21. Murshudov GN, Vagin AA, Dodson EJ. Refinement of macromolecular structures by the maximum-likelihood method. Acta Crystallogr D Biol Crystallogr. 1997; 53:240–255. [PubMed: 15299926]
22. Emsley P, Cowtan K. Coot: model-building tools for molecular graphics. Acta Crystallogr D Biol Crystallogr. 2004; 60:2126–2132. [PubMed: 15572765]
23. Li X, Feng M, Wang Y, Tachikawa H, Davidson VL. Evidence for redox cooperativity between *c*-type hemes of MauG which is likely coupled to oxygen activation during tryptophan tryptophylquinone biosynthesis. Biochemistry. 2006; 45:821–828. [PubMed: 16411758]
24. Li X, Jones LH, Pearson AR, Wilmot CM, Davidson VL. Mechanistic possibilities in MauG-dependent tryptophan tryptophylquinone biosynthesis. Biochemistry. 2006; 45:13276–13283. [PubMed: 17073448]
25. Choudhury K, Sundaramoorthy M, Hickman A, Yonetani T, Woehl E, Dunn MF, Poulos TL. Role of the proximal ligand in peroxidase catalysis - Crystallographic, kinetic, and spectral studies of cytochrome-c peroxidase proximal ligand mutants. J Biol Chem. 1994; 269:20239–20249. [PubMed: 8051115]
26. Smulevich G, Neri F, Willemsen O, Choudhury K, Marzocchi MP, Poulos TL. Effect of the His175-Glu mutation on the heme pocket architecture of cytochrome-c peroxidase. Biochemistry. 1995; 34:13485–13490. [PubMed: 7577937]

27. Garcia-Rubio I, Braun M, Gromov I, Thony-Meyer L, Schweiger A. Axial coordination of heme in ferric CcmE chaperone characterized by EPR spectroscopy. Biophys J. 2007; 92:1361–1373. [PubMed: 17142277]

28. Shin S, Feng ML, Chen Y, Jensen LMR, Tachikawa H, Wilmot CM, Liu A, Davidson VL. The tightly bound calcium of MauG is required for tryptophan tryptophylquinone cofactor biosynthesis. Biochemistry. 2011; 50:144–150.

29. Fulop V, Watmouth NJ, Ferguson SJ. Structure and enyzmology of two bacterial diheme enzymes: cytochrome cd_1 nitrite reductase and cytochrome *c* peroxidase. Adv Inorg Chem. 2001; 51:163–204.

30. Arciero DM, Hooper AB. A di-heme cytochrome-c peroxidase from Nitrosomonas europaea catalytically active in both the oxidized and half-reduced states. J Biol Chem. 1994; 269:11878–11886. [PubMed: 8163487]

31. Foote N, Peterson J, Gadsby PMA, Greenwood C, Thomson AJ. Redox-linked spin-state changes in the di-heme cytochrome c-551 peroxidase from Pseudomonas aeruginosa. Biochem J. 1985; 230:227–237. [PubMed: 2996492]

32. Prazeres S, Moura JJG, Moura I, Gilmour R, Goodhew CF, Pettigrew GW, Ravi N, Huynh BH. Mössbauer characterization of Paracoccus denitrificans cytochrome-c peroxidase. Further evidence for redox and calcium binding-induced heme-heme interaction. J Biol Chem. 1995; 270:24264–24269. [PubMed: 7592634]

33. Desbois A. Resonance Raman spectroscopy of c-type cytochromes. Biochimie. 1994; 76:693–707. [PubMed: 7893820]

34. Hu S, Morris IK, Singh JP, Smith KM, Spiro TG. Complete assignment of cytochrome *c* resonance Raman spectra via enzymatic reconstitution, with isotopically labelled hemes. J Am Chem Soc. 1993; 115:12446–12458.

35. Tu, AT. Raman spectroscopy in biology; principles and applications. John wiley and Sons Inc; New York: 1982. p. 331-337.

36. Shin S, Lee S, Davidson VL. Suicide inactivation of MauG during reaction with O_2 or H_2O_2 in the absence of its natural protein substrate. Biochemistry. 2009; 48:10106–10112. [PubMed: 19788236]

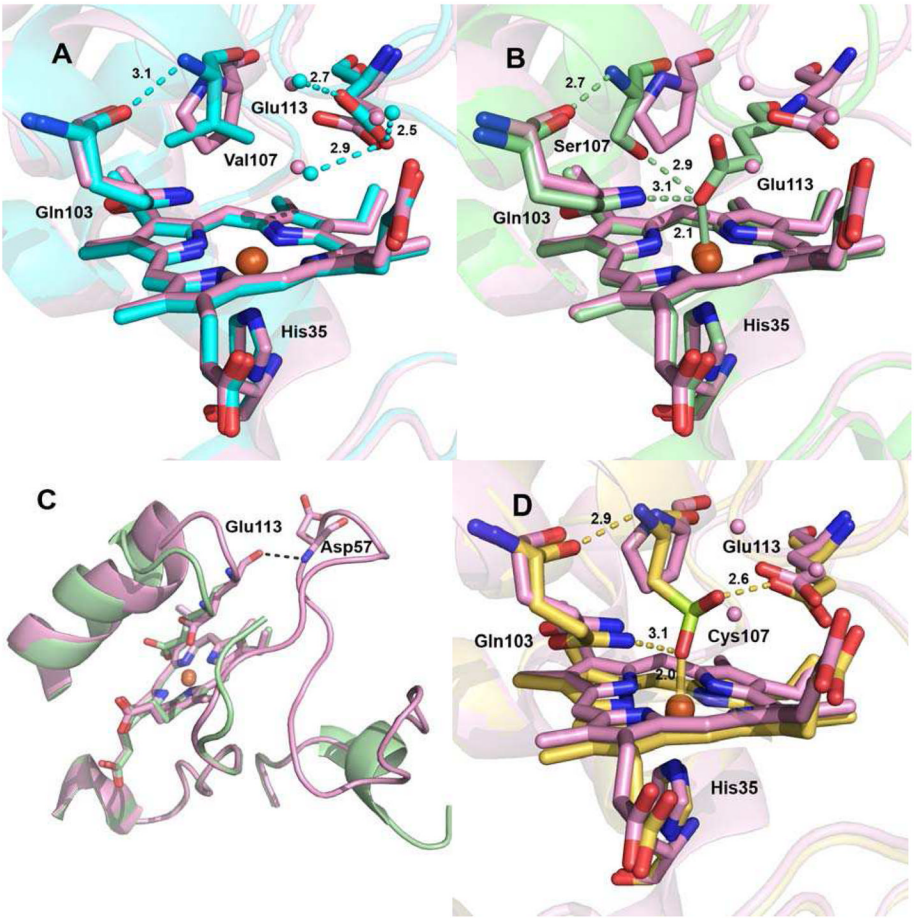

Figure 1.

High-spin heme environment of (A) P107V (cyan) and (B) P107S MauG (green) versus WT MauG (pink, PDB entry 3L4M) in complex with preMADH. (C) Destabilization of a loop structure in P107S MauG (green) versus WT MauG (pink). (D) High-spin heme environment of P107C MauG (yellow) versus WT MauG (pink) in complex with preMADH. Hemes and residues of interest are drawn in sticks colored by atom, with the remaining protein shown in cartoon. The iron is displayed as an orange sphere. Hydrogen bonds are shown as dashed lines. This figure was produced using PyMOL (http://www.pymol.org/).

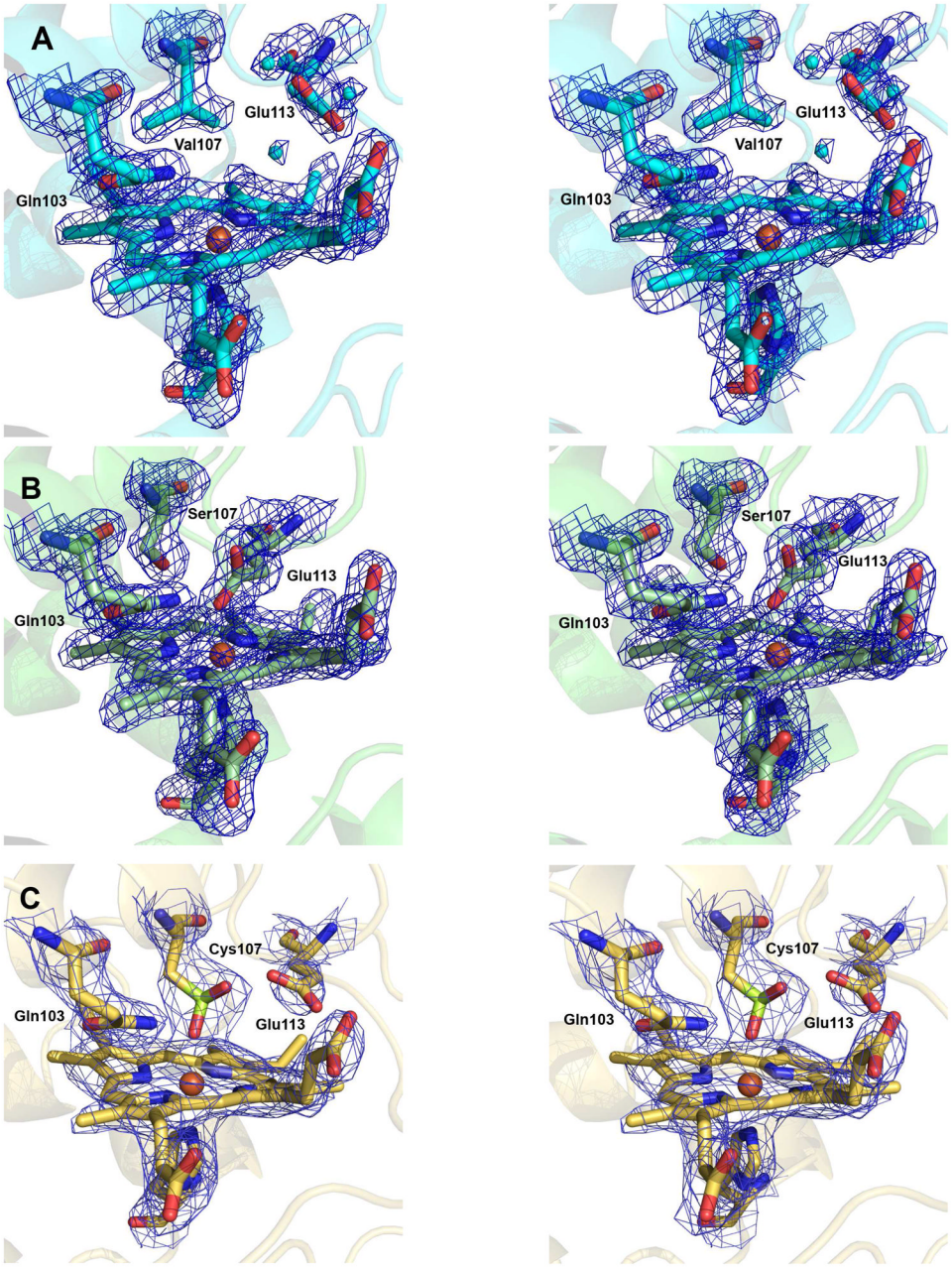

Figure 2.

Stereoviews of electron density for the high-spin heme environment of (A) P107V (cyan), (B) P107S (green), and (C) P107C MauG (yellow) in complex with preMADH. 2Fo-Fc electron density shown as blue mesh contoured to 1.5 σ. Hemes and residues of interest are drawn in sticks colored by atom, with the remaining protein shown in cartoon. The iron is displayed as an orange sphere. This figure was produced using PyMOL (http://www.pymol.org/).

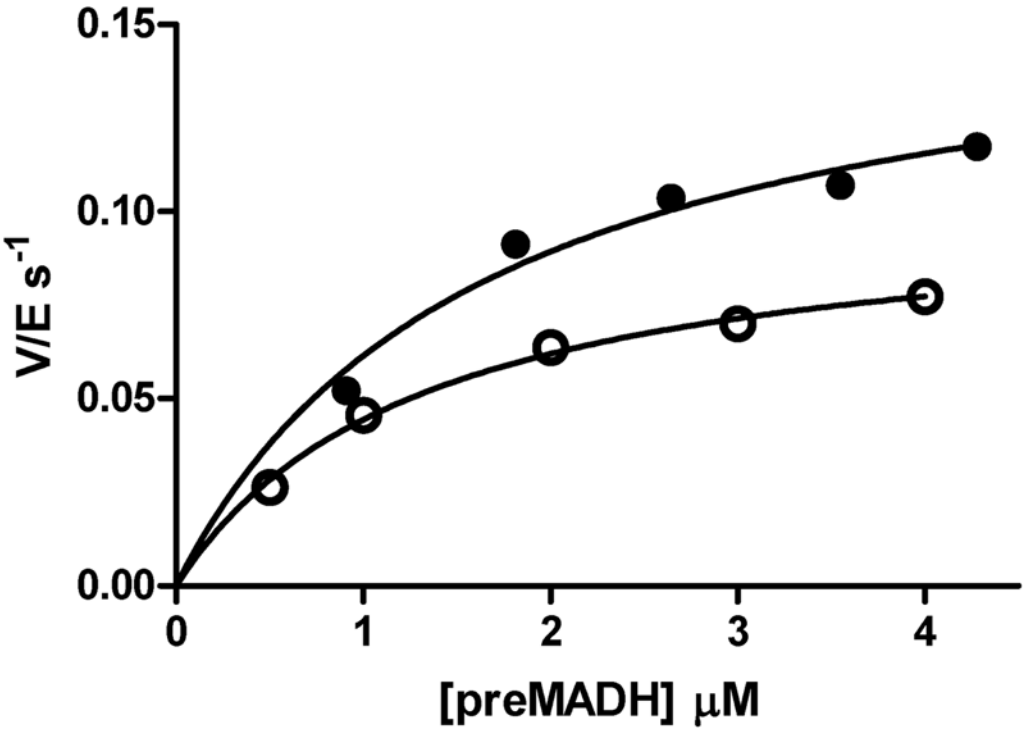

Figure 3.
Steady-state kinetic analysis of P107V MauG-dependent TTQ biosynthesis from preMADH. Data are shown for the reactions catalyzed by P107V MauG (open circles) and WT MauG (closed circles). The lines are fits of the data by eq 1.

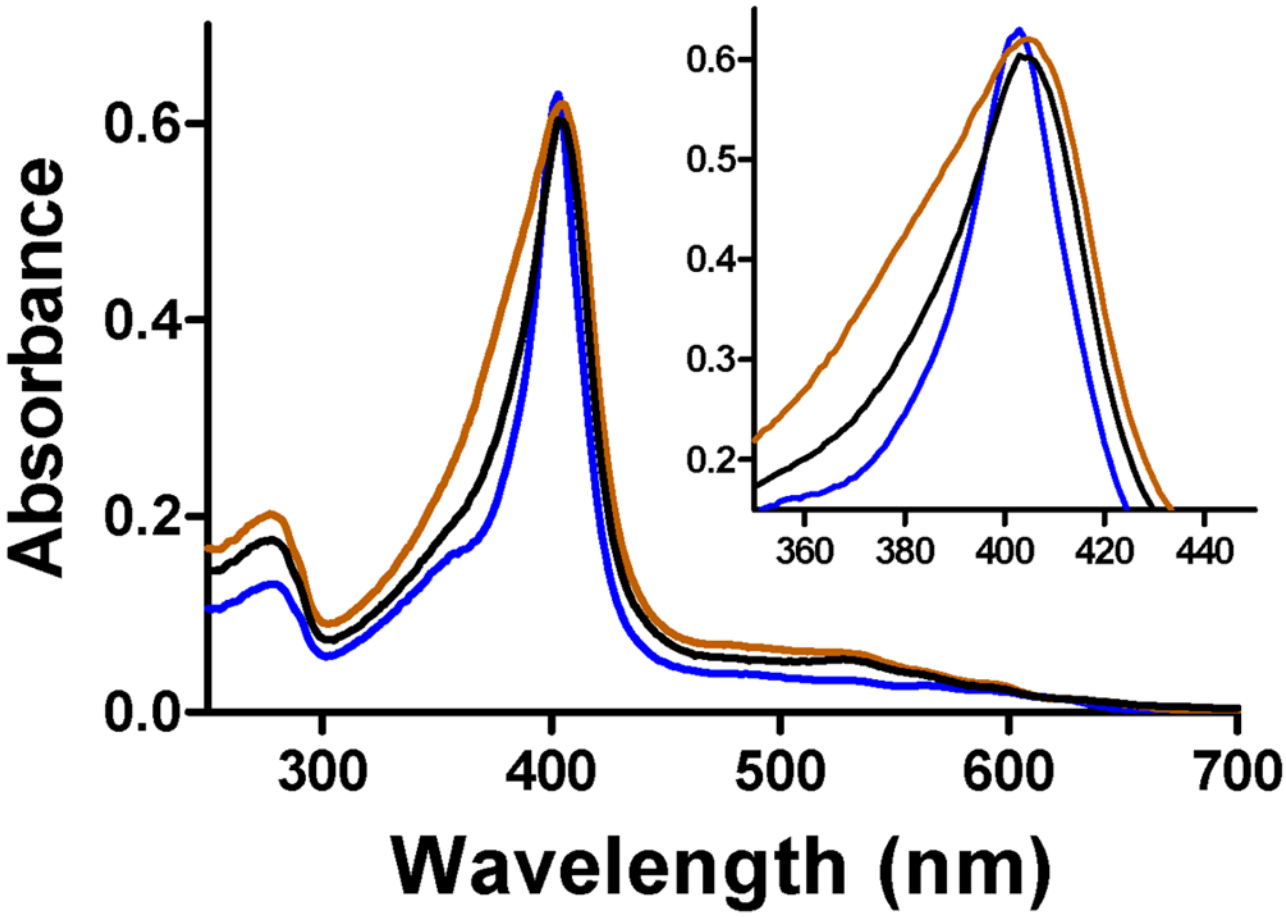

Figure 4.
Visible absorption spectra of WT MauG and Pro107 MauG mutants. Overlay of the absorption spectra of WT MauG (black), P107V MauG (brown) and P107S MauG (blue). The overlay of the Soret peak region of each spectrum is magnified in the inset.

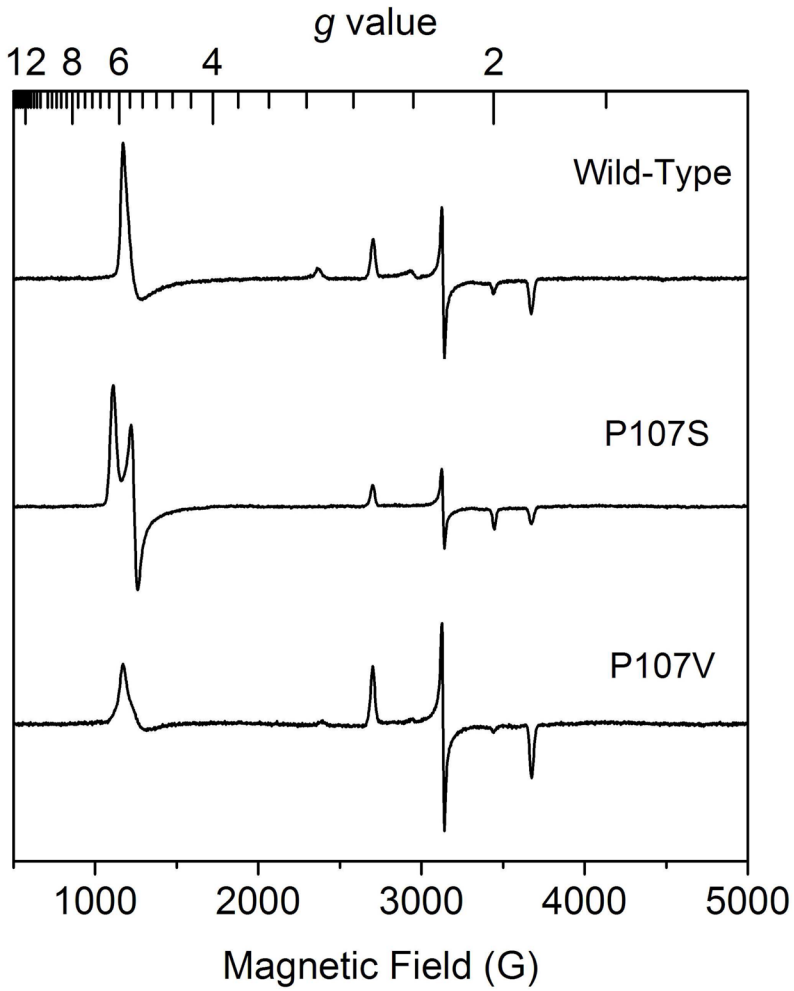

Figure 5.
EPR spectra of WT MauG (top), P107S MauG (middle) and P107V MauG (bottom). EPR parameters for obtaining spectra are as follows: temperature, 10 K; microwave, 1 mW at 9.44 GHz; modulation amplitude, 0.5 mT.

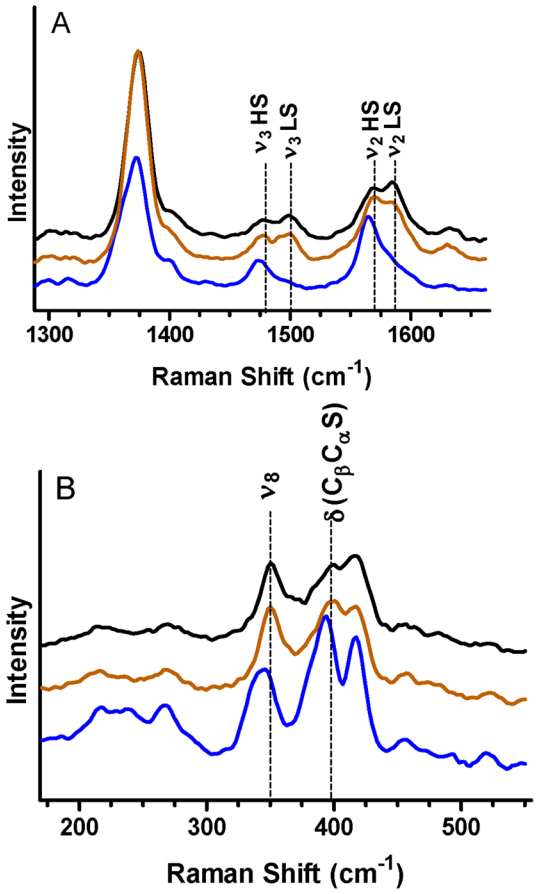

Figure 6.

Resonance Raman spectrum of WT MauG and Pro107 MauG mutants. Overlay of the spectra of diferric WT MauG (black), P107V MauG (brown) and P107S MauG (blue) in the high frequency (A) and low frequency (B) regions. Relevant marker bands are indicated.

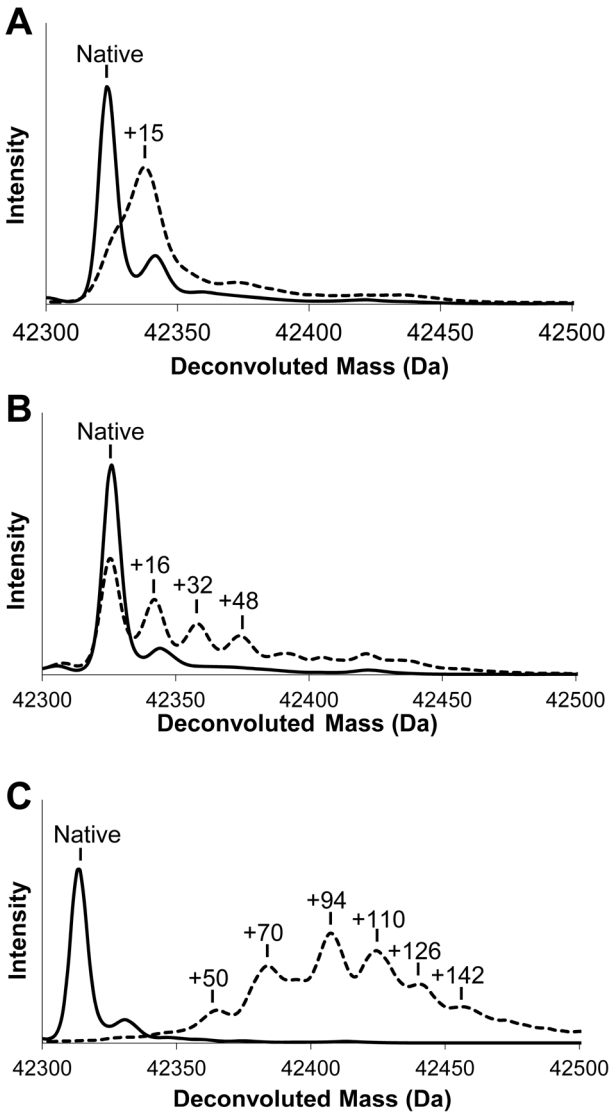

Figure 7.

Deconvoluted mass spectra for 20 μM WT (A), P107V (B) and P107S (C) MauG before (solid line) and after (dashed line) treatment with 200 μM H_2O_2 for one hour.

Table 1

X-ray crystallography data collection and refinement statistics.

Data collection	**P107V MauG-preMADH**	**P107S MauG-preMADH**	**P107C MauG-preMADH**
Space group	*P*1	*P*1	*P*1
Unit cell lengths (Å)	55.6 × 89.0 × 104.8	55.6 × 89.0 × 104.8	55.9 × 88.5 × 107.7
Unit cell angles (°)	67.1, 79.5, 79.7	67.1, 79.5, 79.7	116.2, 91.8, 99.4
Wavelength (Å)	1.03320	1.03320	1.03320
Resolution (Å)[a]	50.00 – 1.87 (1.90 – 1.87)	50.00 – 1.63 (1.66 – 1.63)	50.00 – 2.52 (2.56– 2.52)
Measured reflections	349,049	771,620	127,662
Unique reflections	145,458	208,546	61,043
Completeness (%)[a]	97.0 (86.4)	92.4 (58.6)	97.2 (94.9)
R_{merge} (%)[a, b]	3.9 (11.8)	5.1 (29.2)	6.2 (24.1)
I/σI [a]	21.1 (7.7)	24.2 (2.9)	13.8 (3.4)
Multiplicity [a]	2.4 (2.3)	3.7 (2.6)	2.2 (2.1)
Refinement			
Resolution (Å) [a]	33.89 – 1.86 (1.91 – 1.86)	29.39 – 1.63 (1.67 – 1.63)	47.86 – 2.52 (2.59 – 2.52)
No. reflections; working/test	138,130/7,327	198,077/10,468	56,313/2,992
R_{work} (%)[c]	13.1	14.2	17.4
R_{free} (%)[d]	17.4	18.0	24.3
Protein atoms	13,179	13,106	13,356
Ligand atoms	237	223	198
Solvent sites	2,107	1,966	388
Ramachandran statistics[e]			
Allowed (%)	99.16	99.09	99.11
Outliers (%)	0.84	0.91	0.89
Root mean square deviation			
Bond lengths (Å)	0.025	0.028	0.016
Bond angles (°)	2.09	2.35	1.56
Average B-factor (Å^2)	19.37	22.23	52.77
ESU (Å)[f]; R_{work}/R_{free}	Null/0.113	Null/0.085	2.287/0.314
PDB code	3SVW	3SJL	3SLE

[a] Values in parentheses are for the highest resolution shell.

[b] $R_{merge} = \Sigma_i |I_{hkl,i} - \langle I_{hkl} \rangle| / \Sigma_{hkl} \Sigma_i I_{hkl,i}$, where I is the observed intensity and $\langle I_{hkl} \rangle$ is the average intensity of multiple measurements.

[c] $R_{work} = \Sigma||F_O|-|F_C||/\Sigma|F_O|$, where $|F_O|$ is the observed structure factor amplitude, and $|F_C|$ is the calculated structure factor amplitude.

[d] R_{free} is the R factor based on 5% of the data excluded from refinement.

[e] Based on values attained from refinement validation options in COOT

[f] Estimated standard uncertainties generated for R_{work} and R_{free} in Refmac5.5 in the CCP4i suite.